ESRF	**Experiment title:** **Metal Structures in 4D**	**Experiment number**: MA-558
Beamline: ID11	**Date of experiment**: from: 1/9 2008 to: 30/8 2011	**Date of report**: 15/2/2012
Shifts:	**Local contact(s)**: J. Wright, G. Vaughan	*Received at ESRF:*

Names and affiliations of applicants (* indicates experimentalists):

H.F. Poulsen*, S. Schmidt*, E.M. Lauridsen*, H.O. Sørensen*, D. Juul Jensen, G. Winther, W. Pantleon

Center for Fundamental Research: Metal Structures in 4D, Risoe National Laboratory for Sustainable Energy, Technical University of Denmark, Dk-4000 Roskilde.

In addition we are very grateful to Wolfgang Ludwig, Andy King, and Anatoly Snigirev at ESRF for advice and help during beamtime.

The LTP is defined as comprising Risø lead activities on detector and software developments as well as research projects.

DETECTORS
The main limitation to 3DXRD performance is the nearfield high spatial resolution detector. Due to lack of commercial players, the group has had to develop its own detectors since the beginning of the 3DXRD work. During previous LTPs we have built and installed two high spatial resolution detectors at ID11 with a pixel size of 4.3 microns (Quantix) and of 1.3 microns (Sensicam), respectively. The corresponding FWHMs of the point spread function were 16 microns and 5 microns. It is clear, though, that to achieve a better spatial resolution R&D in detectors is required.

1. Structured Scintillators
Currently, 2D detectors comprising a homogeneous florescence screen coupled by optics to a CCD system are used almost universally at synchrotrons for imaging purposes. However, to obtain a resolution in the 1 micron region, very thin phosphor screens are needed. As a result the efficiency of such detectors are poor (<3% at 50keV), which deteriorate the time-resolution of in situ experiments. As an alternative design we have pursued a structured scintillator concept based on electrochemical etching of pores in silicon. The pores are filled with CsI and serve as waveguides, which collimates the visual light. As a result it becomes possible to use thick – that is efficient – screens without compromising spatial resolution.

Within the first years of the LTP joint work with KTH in Sweden was completed. A new furnace and glove box was been commissioned at Risø dedicated for the filling. As a result screens were produced of size 20x20 mm^2 with a pitch of 4 µm and an aspect ratio of the pores of 15. The efficiency was found to be close to the theoretical value and the homogeneity of the screen was 5% (standard deviation). This work was partly financed also by ID15, who aims at using the scintillators for fast tomography.

More recently, a new collaboration was initiated with MPI in Halle, who are experts in electrochemical etching. Two new batches of structured scintillators were made with much higher aspect ratios. One with a pitch of 2 µm and one with a pitch of 4 µm. The pore height is 100 µm and 150 µm, respectively. The new structured scintillator screens were in 2011 mounted in a new head, which replaces the current head in the 3D detector, see below. First use of the upgraded 3D detector will be after the long winter shutdown between 2011 and 2012.

2. 3D detector

During 2008 and 2009 we have constructed and build a 3D detector – a first of its kind. The 3D detector comprises two semitransparent flourescent screens in series (coupled to two cameras) in the near field and one large area detector (Frelon) in the far field. The camera was integrated with the ID11 beamline operation system and commissioned in summer 2009. In terms of resolution and field-of-view (FOV) both near field detectors surpasses the specifications of the existing ones. The first camera has a FOV of 3mm and resolution FWHM 6µm. The second camera has a FOV of 9mm and a resolution FWHM 12.5µm. The 30µm thick freestanding LuAG:Ce scintillator also leads to an improvement in signal to noise both due to efficiency and purity of the crystal. In addition the combined data set vastly improves options for mapping deformed specimens as ray-tracing can be used. The 3D detector was upgraded twice, first with an improved set of mirrors in March 2010. Now the distortion field is practically negligible which solves a significant issue with the first prototype. As mentioned above the second upgrade was in the second half of 2011, when a new head was mounted with an improved set of structured scintillator screens. **The complete costs of the 3D detector – approximately 140,000 € - is covered by Risø. This funding comes in addition to what was promised in the LTP application.**
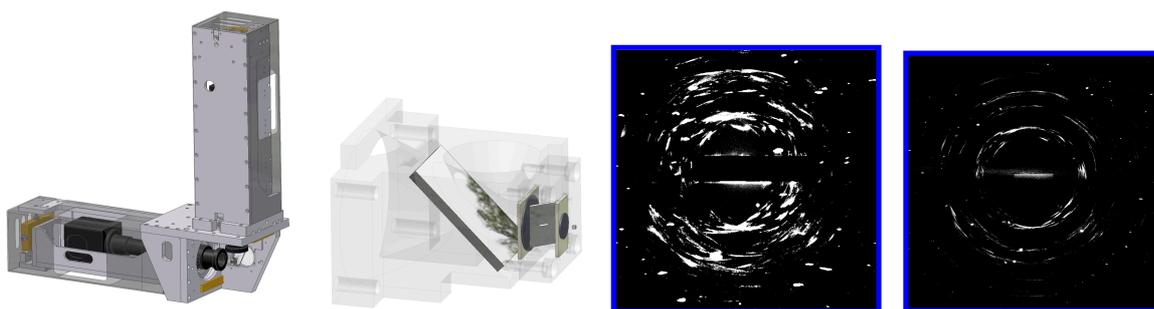
Figure 1. 3D Detector. From right to left: A sketch of the main part of the 3D detector comprising the two near-field screens. A close-up on the head showing the two screens and two mirrors. Experimental data from the two screens – evidently the pattern on the second screen – further from the source - is more reminiscent of a conventional powder diffraction pattern.

The 3D detector has already been used for several beamtimes by external users.

3. Nano-detector

Our group at Risø has invented a new type of 2D detector, the so-called nano-detector. The basic concept of the proposed detector is a strip detector design, as shown in Fig 2. On each side of an X-ray absorbing media parallel lines of electrodes are applied with a 1 μm centre-to-centre pitch. Aiming at single photon detection, the centre-of-mass of the absorption event is determined from the relative intensity of carriers drifting to electrodes in the vicinity of the event. To enable sufficient throughput fast electronics is used.
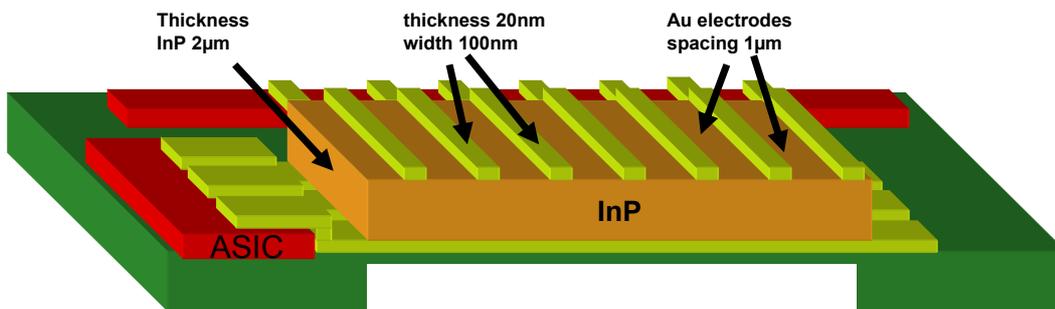
Figure 2. A sketch of the InP based nano-detector (not to scale)

Based on full-scale simulations we find that this detector would have the following unique characteristics

- A spatial resolution of 100 nm or below in the energy range of 8-100 keV (in the hard x-ray end of the range this is more than one order of magnitude better than any existing detector)
- Single photon counting
- The flat area design makes it possible to stack detectors closely to construct a true 3D detector and improve efficiency
- A throughput for synchrotron imaging purposes on the second scale
- An effective area of 1 mm^2

Within a Risø financed proof-of-concept study a primitive version of the detector (with 16 electrodes in stead of 1000) has been made. The clean room work turned out to be a success, but more work is needed in terms of electronics. A number of beamlines at ESRF and elsewhere (PETRA, Max IV, APS, BNL) has expressed an interest in this detector, but funding for continuing this line of work is currently not established.
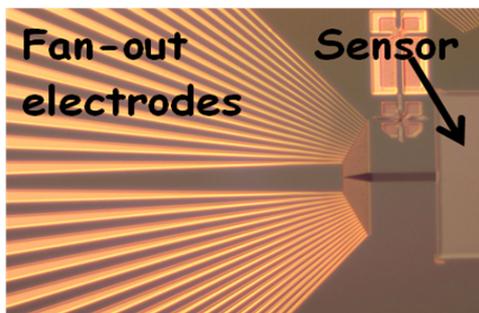
Figure 3. An SEM image of parts of the nano-detector made in the proof-of-concept study. The sensor itself is made by e-beam technology, the fan-out electrodes by UV-beam lithography. The figure is courtesy of the group of K. Yvind at DTU Photonics, Denmark, who is in charge of the clean-room work.

ALGORITHM AND SOFTWARE

1. Mapping of stresses in individual grains

A unique algorithm, FitAllB, has been made for characterization of the grain resolved (type II) stress states in a polycrystalline sample based on monochromatic X-ray diffraction data. The algorithm is a robust 12-parameter-per-grain fit of the centre-of-mass grain positions, orientations and stress tensors including error estimation and outlier rejection. FitAllB is included in the FABLE software package. The algorithm was validated by simulation studies and by an experiment where 96 grains in one layer of IF steel were monitored during elastic loading and unloading. The experiment at ID11 (MA-711) made use of a 69.5 keV beam provided by the Laue-Laue monochromator. The loading was in tension up to 70 N. Very consistent results were obtained, with resolutions for each grain of approximately 10 μm in position, 0.05° in orientation and between 80 and 200 μstrain, depending on strain component. When averaging over all grains a resolution of 10 μstrain was obtained. When adding a nearfield detector to the set-up the spatial resolution could be improved to 2 μm [16, ESRF highlights 2010].

2. 3D orientation imaging

During the previous LTP we developed algorithms for generation of 3D orientation maps of moderately deformed specimens. These were validated by simulations only. During the last two years we have improved the robustness of the GrainSweeper algorithm and succesfully applied it in many ID11 experiments – on deformed Cu, Al and a model material for geophysics, namely NaCl, (the latter was a joint study with S. Piazolo). See also the scientific highlights below.

3. Multigrain Crystallography (indexing, solution & refinement of polycrystals)

Risø, ID11 staff and groups from MPIbpc in Gottingen and University of Oxford have jointly developed "Multigrain crystallography". A major milestone was defined by the completion of the EU grant TotalCrystallography. The final report – which was due end 2009 – can be found at www.totalcryst.dk. The work has progressed according to plan, with the validity of a number of new ideas being demonstrated, typically first by full-scale simulations and then by tests at ID11.

The final result is a series of algorithms for indexing grains, determining diffraction spot intensities and solving crystal structures based on polycrystalline diffraction patterns acquired with conventional crystallography detectors used in crystallography (positioned far from the sample). The algorithms all support arbitrary space groups and unit cell sizes. The main limitation is overlap of the diffraction spots. Hence, the work has been divided into three complementary approaches:

- Approach I (little overlap): For low fractions of overlap a comprehensive data analysis chain was completed during the last LTP. This software has found extensive use in a range of disciplines including photochemistry, pharmacy and structural biology (protein studies). The TotalCryst homepage identifies about 30 publications.
- Approach II (medium overlap): the suggested approach is based on determining a grain orientation distribution function (ODF) for each grain individually from a set of non-overlapping low-index reflections. Spot intensities can then be found by fitting to peak profiles, obtained by forward projection of the ODFs. In collaboration with applied mathematician P.C. Hansen from DTU, Denmark the relevant algorithm has been developed and successfully tested on both simulated and real data [5].
- Approach III (high overlap): A new mathematical representation of orientations has been conceived (the first one in more than 100 years) [8]. This is a real breakthrough as it enables reconstructions of a very large ODF, comprising all grains in the sample, with a high angular

resolution –see task 4 just below. Once the ODF is known one can model the overlap. This is the first step towards dealing with it.

The work on multi-grain crystallography has been summarized in an article, which was selected as one out of five for a special edition of Z. Kristallogr. on the occasion of the centennial for Laue's discovery of x-ray diffracction (H.O. Sørensen *et al.* Z. Kristallogr. (2012) **227**, 63-78) .

4. High resolution Orientation Distribution Function (Super ODF)

The formalism mentioned in 3 for computation of an "super-ODF" implies solving a set of linear equations, $Ax = b$, where A contains the geometry of the orientation space, x is the volume fractions in the ODF, and b is the experimental data. This problem is very large, as the aim is to have the ODF with a resolution of 0.1 degree; however the matrix A is very sparse. Collaboration between Risø and Institute of Mathematical Modeling (both at DTU) has resulted in a full implementation of SODF reconstruction that utilizes multi-core CPUs and many-cores GPUs that accelerates the execution times. So far only simulated data has been tested but the transition to real data is imminent. In Fig 4 shows a 2D slice though the 3D ODF and the capability of capturing smooth as well as sharp features are shown.
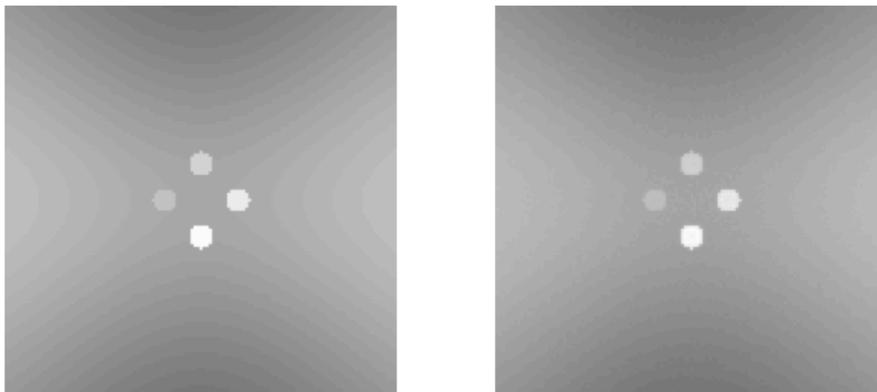
Figure 4. 3D slice through a 3D ODF. Left: Original data. Right: Reconstructed data.

5. 3D grain representations using Laguerre tesselations

A range of 3DXRD based techniques for characterizing individual bulk grains have been developed under the current and previous long term proposals. Whereas some of the developed techniques provide full information on 3D grain shapes, other – faster – techniques are limited to information on crystallography, center of mass and volume. For the latter type of techniques it would still be preferable to gain knowledge of the local grain neighborhood. Hence, an investigation of the validity of using Laguerre tessellations for representations of 3D grain structures based on center of mass and volume information was conducted. In the investigation a beta-titanium alloy was investigated using the Boxscan technique (on ID11) providing information on orientation, center of mass and volume of the individual bulk grains. To validate the results a comparison was made to a 3D grain structure obtained from the same sample using phase contrast tomography (on ID19, MA-90). This investigation confirmed that a) Laguerre tessellations are superior to the well-known Voronoi tessellation when it comes to representing the local topology, and b) the Boxscan technique is capable of spatially resolving embedded bulk grains with a center of mass resolution which is only limited by the mechanics, and as such is independent of detector resolution [15]. These results are illustrated in Fig 5.
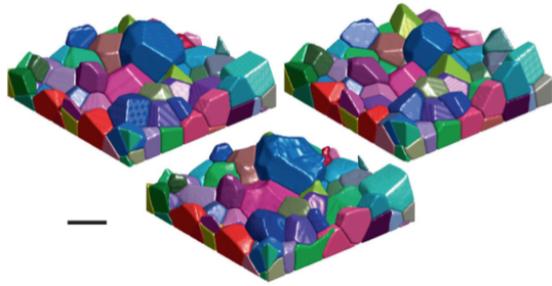
Figure 5.1. Top-left: 3D Laguerre tesselation based on the centers of mass and volumes from the 3D grain structure. Bottom: Segmented 3D grain structure. Top-right: 3D Voronoi tesselation based on the CMS from the 3D grain structure. Scale bar corresponds to 50 mu.
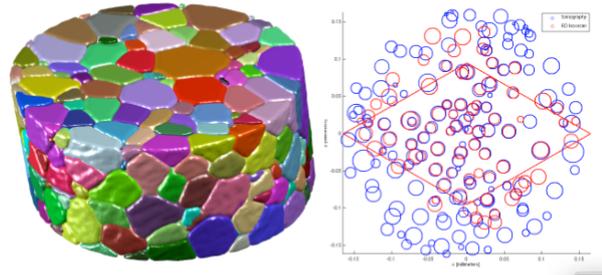
Figure 5.2. Left: 3D beta-tinaium grain structure from phase contrast tomography. Right: Subset of Boxscan and phase contrast tomography results plotted on top of each other. The size of tha circles scale with grain radius. The read diamond is the scanned volume in the Boxscan experiment

6. Software implementation and automisation

For almost a decade, a main goal of the ID11-Risø collaboration has been to integrate the above mentioned 3DXRD type analysis software into a larger beamline computing structure (FABLE) to allow for automated online analysis of 3DXRD type data. The online data analysis is carried out on a cluster of computers, where each data analysis algorithm, ranging from background subtraction to fitting geometrical parameters to mapping grain boundaries in 3D, has been embedded in a device server. In addition, FABLE utilizes a user-friendly GUI interface, allowing new users to quickly setup their experiment and analysis protocol. This task has greatly benefited from regular joint meetings as part of the LTP and the TotalCryst project. More recently, other users and synchrotrons have also contributed, e.g. K. Evans at APS.

Two versions of FABLE were released in 2009 and another in 2011. An International school for demonstrating and teaching FABLE took place at ESRF April 1-3 2009. All programs are freely available on a sourceforge site (http://fable.wiki.sourceforge.net/).

RESEARCH HIGHLIGHTS

1. Direct observation of nucleation events

Nucleation is widely viewed as one of the least understood phenomena in materials science. We have performed a unique recrystallisation study of a 30% cold-rolled Al sample [12]. Initially the local orientations were mapped non-destructively in the as deformed sample using the algorithms mentioned above. Then mapping was done layer-by-layer within a volume of 1000 x 600 x 700 μm^3. Results for one layer are shown in Fig 6. Due to technical issues with the near-field detector at the time this map is actually based on far-field data (using the FRELON detector). For this reason, the spatial resolution in the map is very coarse, of order 20 μm. This however, was sufficient for the study at hand. Next the sample was annealed for 2 min at 320^oC. Following procedures established in the previous LTP new grains were identified from their distinct diffraction signal on the far field detector. Furthermore, their center-of-mass position, orientation and volume could be determined. The signal-to-noise ratio was sufficiently good that the nuclei could be observed provided their size was 1 μm or above.
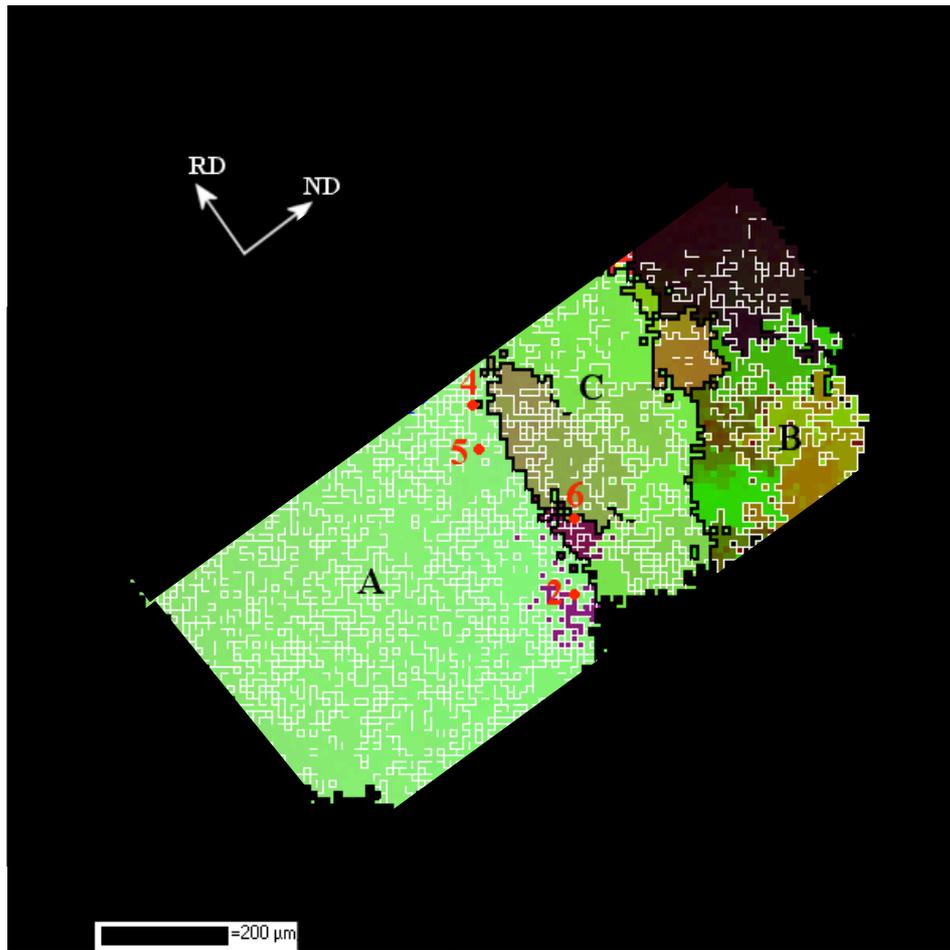
Figure 6. Nucleation in 30% cold rolled Al. Shown is an orientation map for one layer in the as deformed sample. The colours denote orientations. The white and black lines outline regions with misorientations above 2 deg and 15 deg, respectively. Grains A, B and C are identified. Supersposed as red dots are the center-of-mass positions of four new grains, which nucleated in or very close to this layer.

This type of experiment allows for the first time a direct correlation between the orientation and position of the new nuclei with the as-deformed orientation map – cf. Fig 6. Out of six nuclei observed to appear in the interior of the sample, we find that four appear with an orientation that is not present in the deformed state at the position of the nuclei or in the vicinity of this position. This study not only shows that nuclei with new orientations can form spontaneously in the bulk of the material but also allowed the orientation of the nuclei to be related to the type of dislocation structure in the deformed grains

2. Recrystallisation in mildly deformed aluminium

During the recrystallisation of a moderately deformed (30% thickness reduction in cold rolling) aluminium single crystal, the migration of the boundary of an individual grain has been monitored over a large time span using topo-tomography [23]. In topo-tomography, one diffraction vector of the grain of interest is brought parallel to the rotation axis of the stage, in order to obtain different projections of the same diffraction spot representing the grain shape from different viewing angles.

The 3D shape is reconstructed from these projections using a conventional tomography reconstruction algorithm. This technique results in a higher spatial resolution of the grain shape, compared to other non destructive characterisation techniques.

The monitored grain (with orientation {133}<31-2>) is located within the bulk of the deformed single crystal (with orientation {001}<100>). A temperature of about 300 °C has been applied to let the grain grow into the surrounding deformed matrix. Most boundary segments migrated in a stop-go fashion and several protrusions are found. These are similar features as found in earlier experiments with 3DXRD [Schmidt et al., Science 2004;305:229], although in this experiment the grain was growing into a different kind of deformed matrix. Most of the growth of the grain happened through the migration of one planar boundary segment (facet) in the direction almost parallel to the rolling direction.
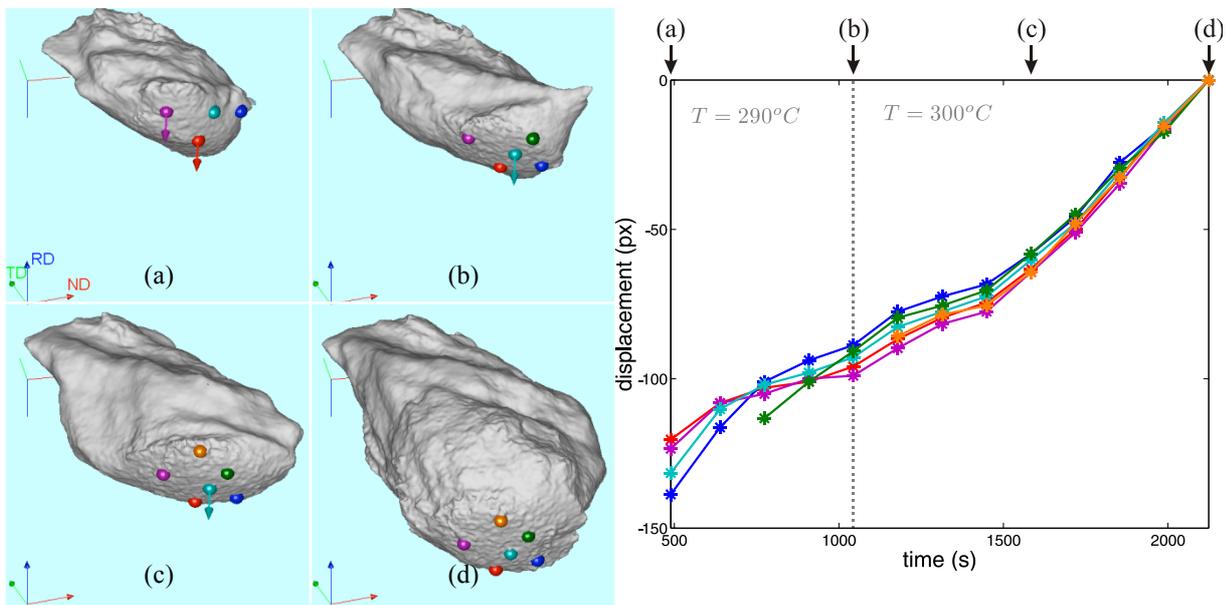
Figure 7. (a)-(d) Snapshots of the reconstructed 3D grain shape at different time steps during its growth. The length of the legs of the tripod corresponds to a length of 42 μm. (e) Displacement of local boundary segments perpendicular to the facet plane as indicated by the coloured markers in (a)-(d).

The formation and migration of facets has been further analysed using a new method that measures the displacements of local boundary segments along parallel lines perpendicular to the facet plane. It has been demonstrated that facets migrate at a constant rate for extended periods of time and that they remain planar during their migration. The crystallography of the analysed facets turned out not to relate to a low-index crystallographic plane. These observations indicate that the local configuration of the substructure has a large influence on the local migration of individual boundary segments.

3. Recrystallization in moderately deformed aluminum

The 3DXRD microscope has been used to investigate the recrystallization behaviour in aluminum cold-rolled to 50% thickness reduction *in situ* [25]. The diffracted intensity from individual recrystallizing grain was recorded on a far-field detector, since the integrated intensity is proportional to the volume of the recrystallizing nuclei, allowing for *in situ* tracking of the growth rate of a large number of individual grains.

This has followed earlier 3DXRD experiments on the same alloy heavier deformed (90% thickness reduction), where it was found that the recrystallization kinetics of individual grains deviate

8

significantly from the mean kinetics usually assumed in models. The new experiment has shown that this behaviour is also observed for the moderately reduced alloy, and so is not a phenomenon caused only by heavy deformation.

At an early stage in the experiment, the temperature was increased. It was found that the increase in the rate of recrystallization caused by the increased temperature of the individual grains varied significantly. By considering the growth rate of an individual grain before - and after the temperature increase, a "grain-averaged activation energy", linking the growth rate of an individual grain to temperature, was derived for 793 individual grains. It was found that the grain-averaged activation energies constituted a very broad distribution,and represent the first large-scale experimental study of activation energies of individual bulk grains during recrystallization.
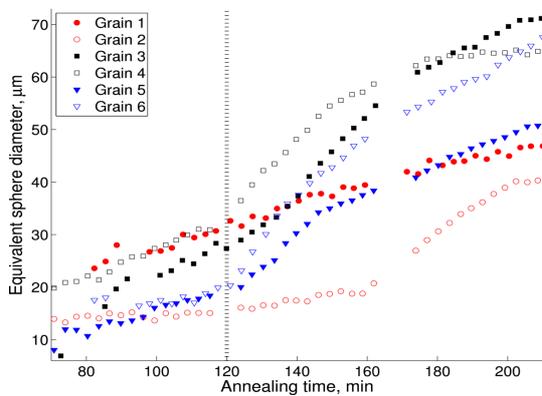
Figure 8. Growth rate of individual grains in aluminium during recrystallization. The vertical line marks when the temperature was increased.
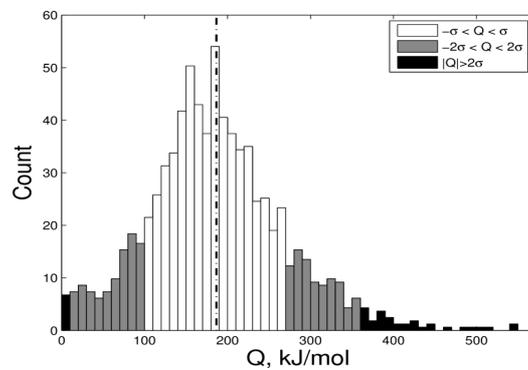
Figure 9. The distribution of grain-averaged activation energies of individual grains in aluminum during recrystallization. The vertical line marks the average, which is found to be consistent with values reported for bulk recrystallization.

4. Grain Growth in Al-Mg

A grain growth experiment in the new hutch has been performed in collaboration with C. Krill (MA-263). Due to instrumental issues and mutual scientific interests of the two groups it was decided to merge the MA-263 beamtime with 5 days of LTP beamtime on this study. A cylindrical Al specimen with 1.5 mm diameter was mapped within a complete 1 mm in height in three time steps, see Fig 10. Reconstructions for the last step (966 grains) has been performed using the GrainSweeper program. The reconstruction of the two other steps are in progress, and it found that the time steps are ideal with on average ~15% growth between annealings. Hence, we feel certain that this data set will be able to test a range of very basic assumptions in grain growth.
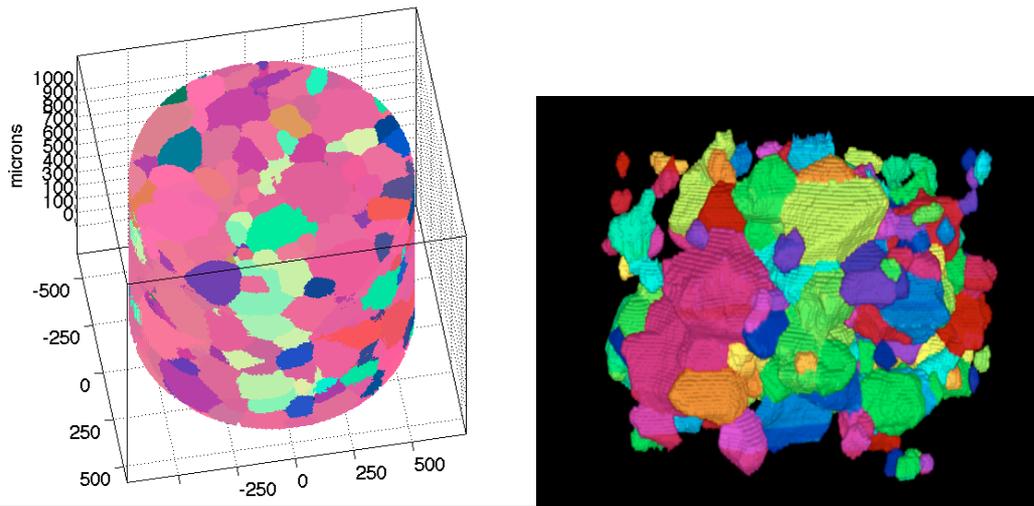
Figure 10. 3D grain reconstruction of grain growth experiment with C. Krill. Right: The microstructure after the last annealing is shown. Left: Bulk grains.

5. Grain growth kinetics in Ti β-21S

In collaboration with Navy Research Lab in Washington, Northwestern University in Chicago and ID19 staff: W. Ludwig, A. King, S. Rolland, the Risø group has established an alternative to 3DXRD for 3D grain mapping based on the use of phase contrast tomography. The technique has the advantage of a better spatial resolution – currently 1 μm – but is restricted to very few materials. More specifically focus is on β-21S Ti, where the low-temperature phase is used to decorate the boundaries of the grains of the high temperature phase. By repeated annealing at high temperature (evolution of grain structure) and cooling to intermediate temperature (mapping of grains) one can use this approach to study the basics of coarsening. The bulk of the experiments have been performed at ID19 and within the project MA-90.

The main results of these studies are summarized in Fig 11. For the first time it has been possible to make a 3D movie of the coarsening (of in this case approx 1000 grains) and compare it directly to a 3D simulation based on the same initial microstructure. A detailed analysis shows that the main discrepancy between experiment and model is due to the model being an isotropic phase field model. The partners at Northwestern are working on novel anisotropic models, but to compare these to experiments, it is required to know the orientation of each grain. Such information cannot be derived from phase contrast tomography. Hence, as part of the current LTP MA-558 we have performed 3DXRD on the same samples at the beginning and end of the annealing study. The work is currently in print.
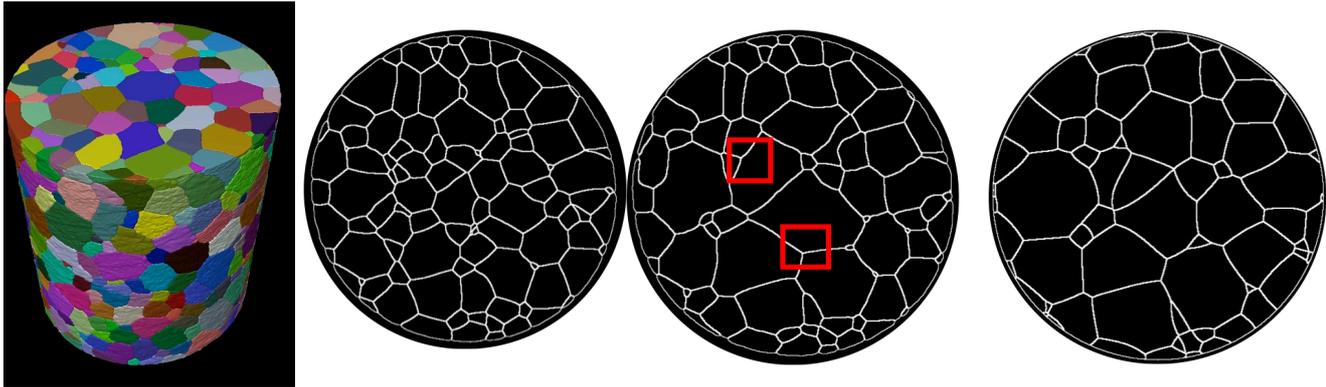
Figure 11. Coarsening of Ti. Left: experimental 3D grain structure before annealing. Colors only serve to visualize grains. Middle: one layer in the microstructure before annealing and after annealing. Right: same layer after annealing as simulated by an isotropic phase field simulation. One of the main differences between experiment and simulation is marked by the red boxes: in the experiment dihedral angles vary substantially, while they are fixed at 120 degrees in the simulations.

6. Slip amplitude maps

An ultimate aim in plasticity research is to identify *in situ* the active local slip systems and to correlate this to a 3D map of the microstructure. Such information would enable very detailed comparisons with modeling and provide key insight into e.g. grain interaction. We propose to enable such studies by working on fcc model systems comprising marker particles, which can be identified and tracked during the loading. For such systems, we argue that the slip amplitudes can be derived directly – and in 3D – by a combined mapping of the plastic displacement gradient strain (based on tomography) and the local rotation map (based on 3DXRD). A first study of this kind was performed on an Al/Pb alloy with approx 2 μm Pb particles. In collaboration with M. Kobyashi and H. Toda from Toyohashi University and K. Uesugi and A. Taheuchi from SPring-8, the 3DXRD study was performed at ID11 and the tomography part at BL47 at SPring-8. The data analysis for the two individual studies have been completed, see Fig 12 and 13. We are currently working on deriving the final slip amplitude map.
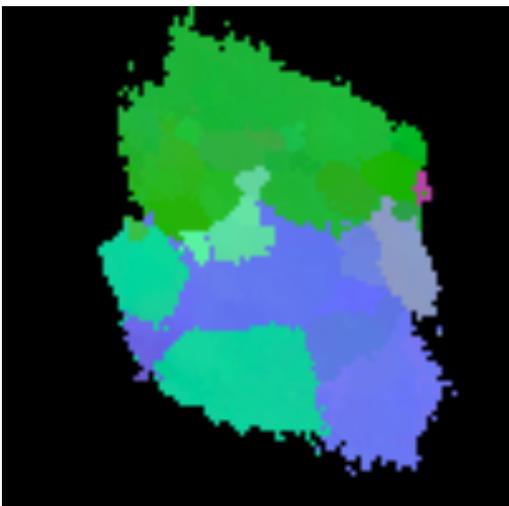
Figure 12. One layer of 10% tensile deformed sample reconstructed by GrainSweeper. Clear grain breakup is seen.
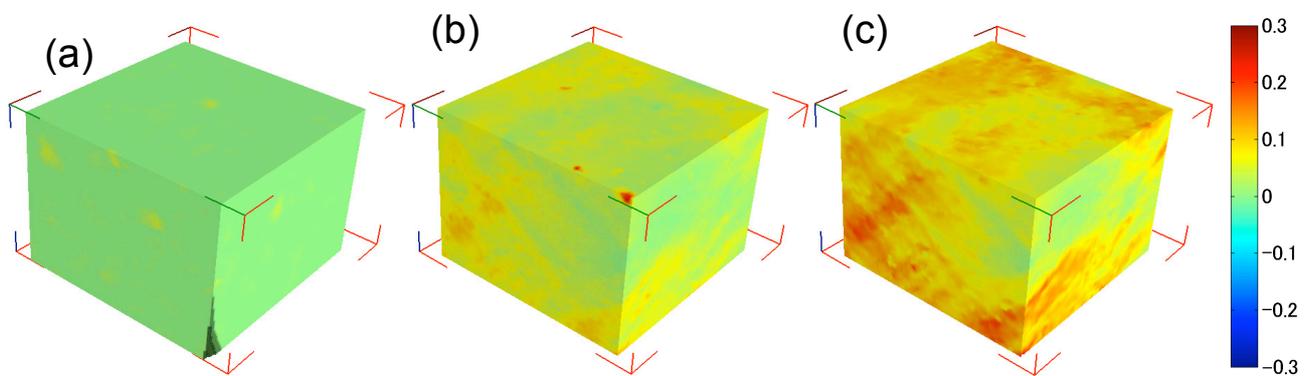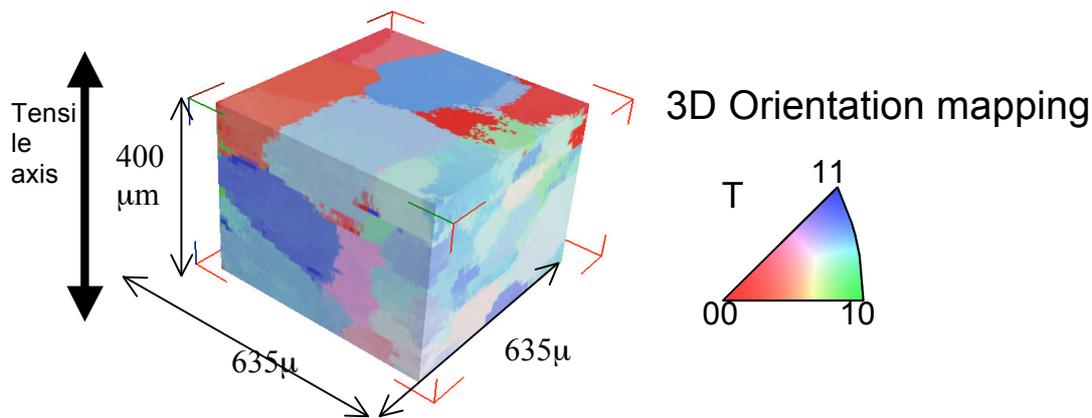
Figure 13. Plastic deformation of Al with Pb particles. Shown is the central part of the tensile specimen. Above: 3DXRD map of the undeformed sample. Colors denote orientations as defined by the stereographic triangle. Below: plastic strain maps from the same volume at a) 0%, b) 5% and c) 10% tensile loading. The colors symbolise the axial strain as shown to the right (red is tension). The resolution of the plastic strain maps is approx 20 μm.

7. 3DXRD measurements of lattice rotations in tensile deformed IF steel

The positions and orientations of almost 2000 grains in a volume of $0.7 \times 0.7 \times 1$ mm^3 within a recrystallised interstitial free steel sample have been measured using 3DXRD [20]. The sample was tensile deformed in steps to 9% strain. 75 % of the grains could be identified once more at 3% strain. At 9% strain the sample was thinned down to reduce overlap of diffraction spots. In a smaller volume that contained 207 grains at 0% deformation, 158 could be identified again at 3% and 107 at 9%. Centre of mass positions of the identified grains at 3 and 9% are shown in Fig 14.
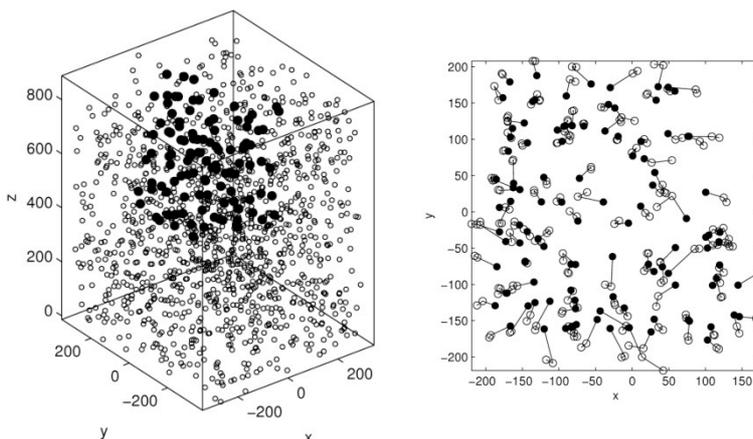
Figure 14. Left) Plot of the positions of the matched grains. Grains that could be tracked from 0% over 3 % to 9% are marked by filled symbols, while the symbols for grains that could only be followed to 3% are open. Right) The 107 grains tracked from 0% over 3% to 9% (filled) viewed along the tensile axis. The unit on the axes is μm.

12

The observed lattice rotations have been analysed qualitatively (see Fig 15). They show an orientation dependence similar to that previously observed in aluminium, but with reversal of the rotation direction as expected when going from face centred to body centred cubic crystal symmetry.

Figure 15. Stereographic triangles showing lattice rotations. The line represents the rotation path and the dot corresponds to the orientation at the maximum deformation. Left) Rotation from 0% to 3% deformation. Right) Rotation from 0% over 3% to 9% deformation.
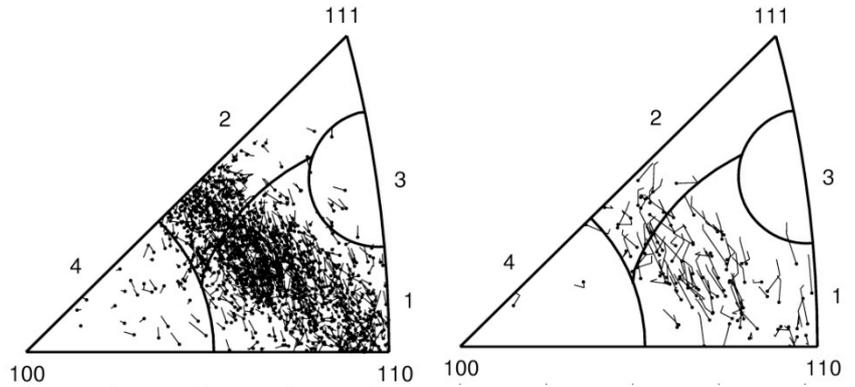
8. Grain-resolved elastic strains in deformed copper measured by 3DXRD

The grain-resolved elastic strains in 1118 randomly oriented grains embedded in a polycrystalline copper sample were measured by *in situ* 3DXRD in the undeformed state and at a plastic strain of 1.5 % while the sample was under tensile load. For each grain the centre-of-mass position was determined with an accuracy of 10 μm, the volume with a relative error of 20 %, the orientation to 0.05° and the axial strain to 10^{-4}. The spatial distribution of axial strain is shown in Fig 16.
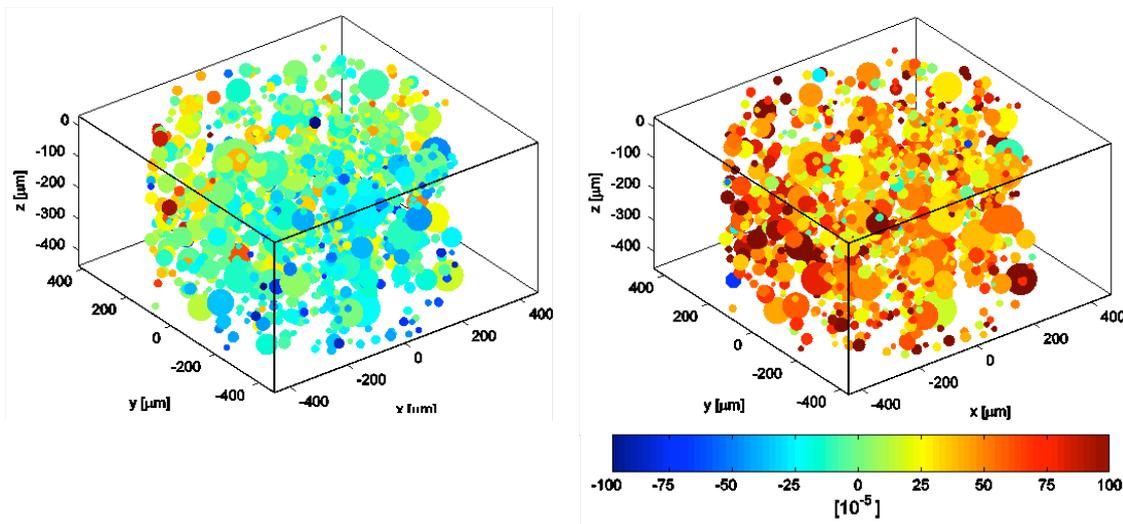
Figure 16. Centre-of-mass positions of 1118 grains in the mapped section of the cylindrical polycrystalline Cu sample plastically deformed under tensile load (along z) colour coded according to: Left) residual axial strain in undeformed sample, and Right) absolute axial strain at maximum load. The diameters of the spheres represent the relative grain sizes.

To eliminate any influence of the free surface the analyses of the effects of grain orientation were restricted to the 871 bulk grains. The elastic strain along the tensile direction was found to exhibit a grain orientation dependence with grains within 20° of <100> carrying a 50% larger strain, cf. Fig 17.
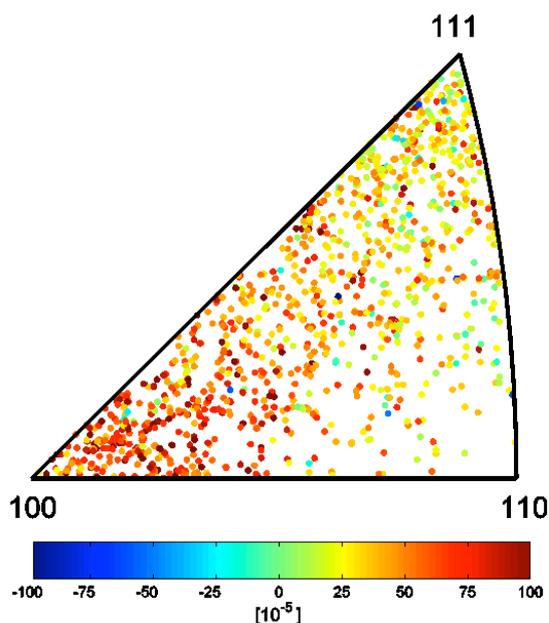
Figure 17. Stereographic triangle showing the orientation distribution of the 871 mapped bulk grains, colour coded according to their axial strain responses.

WORK RELATED TO THE NANOSCOPE

Substantially work was invested during the three years in developing the technology required for the socalled nanoscope – this involved LTP as well as in house beamtime. The aim is have a hard x-ray nano-probe for diffraction, first of its kind (as it is operating above 25 keV). The main obstacles turned out to be quality of focusing schemes and stability issues. With respect to the focusing at the end of 2010 a stable 2D beam of 85 nm was generated using an ad hoc set-up in experimental hutch EH3 and using a combination of compound refractive lenses – a collaboration with A. Snigirev from the ESRF ISDD division.
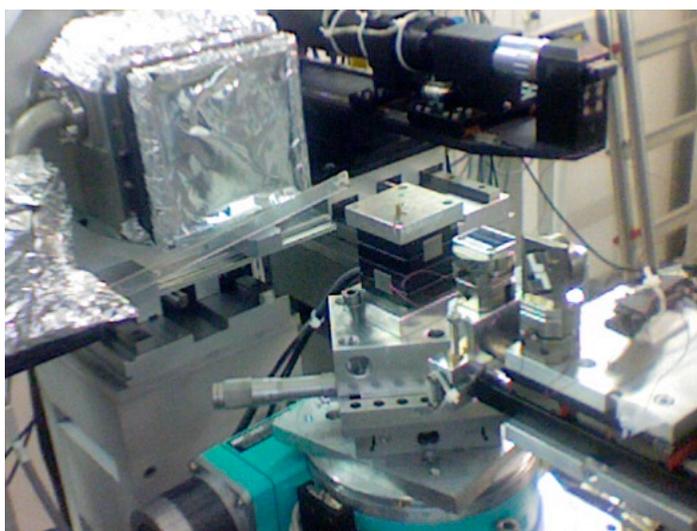
In order to overcome the stability problems in 2011 focus was on building a socalled **interim nanoscope.** This new station – placed at the end of EH3 – is essentially a hard x-ray optics platform. The platform has the required stability and enables a mounting of three detectors simultaneously. As shown in the photo above, on top of the platform in an ad hoc fashion

goniometers for CRL optics and the sample are placed. Two sets of 1D Si compound refractive lenses (CRLs) are used. These have small shape errors and also have the advantage in comparison to 2D lenses that a larger demagnification can be used in the horizontal plane, compensating for the anisotropic source size. The use of coupled 1D lenses also allows the elimination of any astigmatism. This allows a more or less isotropic focus size to be obtained.

The funding for the nanoscope provided in part by ID11, in part by Risø. **This funding is in excess of what was promised in the LTP propsoal.**

The interim nanoscope was succesfully commissioned and used for first 3D grain mapping purpsoes in two beamtimes: June 2011 and November 2011. Due to the delays outlined above it was not possible to pursue the proposed experimental program on nano-metals within the time frame of LTP MA-558. This work will, however, be continued in the context of a European Advanced Grant (grant holder: Henning Friis Poulsen) and ESRF long term project LTP MA1317. We refer to the annual report on MA1317 for details on the commissioning and 3D grain mapping.

Peer-Reviewed International Publications of research related to the LTP MA-558

1. Ludwig, W., Schmidt, S., Lauridsen, E.M. and Poulsen, H.F. *J. Appl. Cryst.* (2008) **41,** 302-309
2. Olsen, U.L., Schmidt, S. and Poulsen, H.F. *J. Synchrotron Rad.* (2008), **15**, 363-370
3. Schmidt, S., Olsen, U.L., Poulsen, H.F., Sørensen, H.O., Lauridsen, E.M., Margulies, L., Maurice, C. and Juul Jensen, D. *Scripta Mater.* (2008) **59,** 491-494
4. Poulsen, H.F., Nielsen, S.F., Olsen, U.L., Schmidt, S. and Wright, J. *Proc. Risø international symposium on materials science* (2008), 101-122.
5. Hansen, P. C., Sørensen, H. O., Sükösd, Z. and Poulsen, H. F. *SIAM J. Imag. Sci.* (2009) **2**, 593-613
6. Kulshreshth, A. K., Alpers, A., Herman, G. T.. Knudsen, E., Rodek, L. and Poulsen, H. F. I*nverse Problems and Imaging* (2009) **3**, 69-85
7. Juul Jensen, D.; Schmidt, S., *Materials Transactions* (2009) **50**, 1655-1659.
8. Kazantsev, I.G.; Schmidt, S.; Poulsen, H.F. *Inverse Problems* (2009) **25,** Article no. 105009
9. Ludwig, W.; King, A.; Reischig, P.; Herbig, M.; Lauridsen E.M.; Schmidt, S.; Proudhon, H.; Forest, S.; Cloetens, P.; du Roscoat, S.; Rolland, S.; Buffiere, J.Y.; Marrow, T.J.; Poulsen, H.F. *Mater. Sci. Eng. A* (2009) **524**, 69-76.
10. Ludwig, W.; Reischig, P.; King, A.; Herbig, M.; Lauridsen, E.M. ; Johnson, G.; Marrow, T.J.; Buffiere, J.Y., Rev. Sci. Instr. (2009) 80(3), Article no. 033905
11. Olsen, U.L.; Schmidt, S.; Poulsen, H.F.; Linnros, J.; Yun, S.H.; Di Michiel, M.; Martin, T. *Nucl. Instr. & Meth. Phys. Res. A* (2009) **607**, 141-144
12. West, S.; Schmidt, S.; Sørensen, H.O.; Winther, G.; Poulsen, H.F.; Margulies, L.; Gundlach, C.; Juul Jensen, D., *Scripta Materialia* (2009) **61**, 875-878 .
13. Oddershede, J.; Schmidt, S.; Poulsen, H.F.; Margulies, L.; Wright, J.P.; Moseicki, M.; Reimers, W., *Proceedings 30. Risø Symposium Sept. 7-11* (2009) 277-283
14. King, A.; Herbig, M.; Ludwig, W.; Reischig, P.; Lauridsen, E.M.; Marrow, T.; Buffière, J.Y., Nucl. Instr. Meth. Phys. Res. B (2010) 268, 291-296.
15. Lyckegaard, A.; Lauridsen, E.M.; Ludwig, W.; Fonda, R.W.; Poulsen, H.F., Adv. Eng. Mater. online Nov. 16th 2010 with DOI: 10.1002/adem.201000258
16. Oddershede, J.; Schmidt, S.; Poulsen, H.F.; Sørensen, H.O.; Wright, J.; Reimers, W., J. Appl. Cryst. (2010) 43, 539-549.
17. Alpers, A.; Herman, G.T.; Poulsen, H.F.; Schmidt, S., Optical Society of America. Journal A: Optics, Image Science, and Vision 27(9) (2010), 1927-1937.

18. Lyckegaard, A.; Alpers, A.; Ludwig, W.; Fonda, R.W.; Lauridsen, E.M., Proceedings of the International Risø Symposion on Materials Science (2010), 329-336.
19. Oddershede, J.; Schmidt, S.; Poulsen, H.F.; Reimers, W., Mater. Sci. Forum (2010) 652, 63-69.
20. Oddershede, J.; Wright, J.P.; Margulies, L.; Huang, X.; Poulsen, H.F.; Winther, G., Proceedings of the International Risø Symposion on Materials Science (2010), 369-374.
21. Poulsen, H.F.; Ludwig, W.; Lauridsen, E.M.; Schmidt, S.; Pantleon, W.; Olsen, U.L.; Oddershede, J.; Reischig, P.; Lyckegaard, A.; Wright, J.P.; Vaughan, G., Proceedings of the International Risø Symposion on Materials Science (2010), 101-119.
22. Poulsen, S.O.; Lyckegaard, A.; Oddershede, J.; Lauridsen, E.M.; Gundlach, C.; Curfs, C.; Juul Jensen, D., Proceedings of the International Risø Symposion on Materials Science (2010), 391-396.
23. Van Boxel, S.; Schmidt, S.; Ludwig, W.; Zhang, Y.B.; Sørensen, H.O.; Pantleon, W.; Juul Jensen, D., Proceedings of the International Risø Symposion on Materials Science (2010), 449-456.
24. Vaughan, G.B.M.; Wright, J.P.; Bytchkov, A.; Curfs, C.; Gundlach, C.; Orlova, M.; Erra, L.; Gleyzolle, H.; Buslaps, T.; Götz, A.; Suchet, G.; Petitdemange, S.; Rossat, M.; Margulies, L.; Ludwig, W.; Snigirev, A.; Snigireva, I.; Schmidt, S.; Sørensen, H.O.; Lauridsen, E.M.; Olsen, U.L.; Oddershede, J.; Poulsen, H.F., Proceedings of the International Risø Symposion on Materials Science (2010), 457-476.
25. Poulsen, S.O.; Lauridsen, E.M.; Lyckegaard, A.; Oddershede, J.; Gundlach, C.; Curfs, C.; Juul Jensen, D., Scripta Mater. (2011) 64, p. 1003-1006
26. Lyckegaard, A.; Lauridsen, E.M.; Ludwig, W.; Fonda, R.W.; Poulsen, H.F. Advanced Engineering Materials. (2011), 13(3), 165-170
27. Syha, M.; Rheinheimer, W.; Bäurer, M.; Lauridsen, E.M; Ludwig, W.; Weygand, D.; Gumbsch, P. Scripta Mater. (2011), 66, 1-4.
28. Aagesen, L.K.; Fife, J.L.; Lauridsen, E.M.; Voorhees, P.W. Scripta Mater. 64 (2011), 394–397
29. Oddershede, J.; Schmidt, S.; Poulsen, H.F; Margulies, L.; Wright, J.; Moscicki, M.; Reimers, W.; Winther, G. Materials Characterization (2011) 62, 651-660.
30. Paithankar K.S; Sørensen, H.O.; Wright, J.P.; Schmidt S., Poulsen H.F.; Garman E.F. Acta Cryst. D (2011) 67, 608-618.
31. Sørensen, H.O.; Schmidt, S.; Wright, J.P.; Vaughan, G.B.M.; Techert, S.; Garman, E.F.; Oddershede, J.; Davaasambuu, J.; Paithankar, K.S.; Gundlach, C.; Poulsen, H.F. Z. Kristallogr. (2012) 227, 63-78

Reviews for general Audience

1. Juul Jensen, D. Offerman, S.E. and Sietsma, J. *MRS Bulletin* (2008) **33**, 621-629.
2. Thornton, K. and Poulsen, H.F. *MRS Bulletin* (2008) **33**, 587-595

Book chapters

1. Poulsen, H.F. *Three dimensional X-ray diffraction* In: Banhart, J., Ed.: *Advanced tomographic methods in materials research and engineering,* pp 249-277 (Oxford University Press, 2008, New York)
2. Poulsen, H.F. Ludwig, W. and Schmidt, S. *3D X-ray diffraction microscope.* In: Reimers, W.,Pyzalla, A.R., Schreyer, A.,Clemens, H., Ed.: *Neutrons and synchrotron radiation in engineering materials science - from fundamentals to material and component characterization,* pp 335-351 (Wiley-VCH, 2008, Weinheim)